Wigner lattice between two dielectric slabs: Image potential and Casimir effect

Z. Lenac
Department of Physics, University of Rijeka, 51000 Rijeka, Croatia

Ž. Crljen
Institute Rudjer Bošković, P.O. Box 180, 10002 Zagreb, Croatia and Department of Physics, Faculty of Sciences, University of Split, 21000 Split, Croatia

(Received 19 February 2012; published 29 August 2012)

We analyze a model of electron lattice between two metallic or polar dielectric slabs. Typically, the electrons are confined on a thin helium layer above a metallic slab and form, under given circumstances, the Wigner lattice. We assume that another slab is placed above the electron layer at a distance away to have negligible influence on basic properties of the Wigner lattice. Here we want to analyze the total force acting on the lattice electrons as well as the total force acting between the metallic (or dielectric) slabs. From the classical electrodynamics one can determine the image potential and calculate corresponding forces. In the quantum electrodynamics, fluctuations of the electromagnetic field will add in attraction between the slabs due to the Casimir effect. We calculate and compare those two forces on the slabs within the same model, since they are an explicit manifestation of the same field. We found out that the resulting forces can be of comparable strengths in the appropriate setup.

DOI: 10.1103/PhysRevA.86.022524 PACS number(s): 31.30.jh, 42.50.Ct, 12.20.−m, 73.20.Mf

I. INTRODUCTION

In the last few years there has been growing interest in the Casimir effect [1], often in connection with various micro- and nanotechnologies. The needs for miniaturization of electromechanical systems have prompted the advances in experimental tools that have made it possible to measure forces at submicron separation with a high accuracy [2]. In such examples the Casimir forces, that are normally neglected in macro systems, have to be taken into account. At separations below 100 nm, they are rather strong and comparable to electrostatic forces corresponding to voltages up to 1 V [3]. In the nanotechnology of carbon nanotubes (CNTs) the knowledge of the forces between CNT and substrate material are of great importance for the design of new materials. New phase-change materials and shape of the boundaries can modify the strength [4] and even the sign [5,6] of the Casimir forces, which opens a way for a force transmission without mechanical contacts.

A deeper knowledge of the Casimir forces could provide new insights and design alternatives that might lead to a breakthrough in future micro- and nanoelectromechanical machines [4,5]. Even if no electric currents are involved, there are often electric charges present and for the proper functioning of the machines, the electrostatic properties should be accounted for. Dielectric or metallic plates are typically involved in such devices and forces because the image potential should be considered besides the Casimir forces. In order to investigate a cumulative effect of the image and the Casimir force, we consider in this paper an idealized model consisting of an electron lattice between dielectric slabs. It is not *a priori* clear how an electron density (i.e., a lattice parameter) or a lattice position between the slabs will influence, e.g., a stability of the lattice or a force on the dielectric slabs. We shall take into account the influence of these "image" parameters together with a slab separation (which essentially determines the Casimir force) when evaluating the total force between the slabs. The precise knowledge of the total force is of particular importance in order to account for it properly in the design of novel devices.

Our system consists of two parallel, semi-infinite, polar dielectric or metallic slabs. We fill in to some height the liquid He in between the slabs and put the layer of electrons on top of the He surface [7]. The thickness of the He layer should be above 3 nm in order to prevent electrons from penetrating into the dielectric substrate [8]. We assume that the electron concentration n_e is not very high ($n_e < 10^{13}\,\mathrm{cm}^{-2}$) [9], so that the electrons will form a quasi two-dimensional (2D) Wigner lattice [10,11]. We also assume the temperature close to zero to avoid any excitation [12] or phase transition [13] of lattice electrons. Such a system is well known and much discussed regarding the properties of the Wigner lattice (eigenfrequencies, ground-state energy, excitations, phase transition), but here we want to analyze in detail the image force on electrons configured in between two dielectric or metallic slabs as well as the interaction between the slabs.

In the *classical* approach we start with a point charge e at a distance z above a semi-infinite perfect conductor. In order to provide perfect screening, the charge e will induce an image charge $-e$ at a distance z below the conductor surface, thus leading to the charge-conductor interaction (image potential) $W^{\mathrm{im}}(z) = -e^2/4z$. If we put more point charges above the conductor slab, besides the direct interaction between the charges, each charge will interact with its own image and with all images induced by other charges. Let us add another perfect conductor above the charges, so that each charge will induce its "own" images at both conductor slabs. In order to ensure complete screening, the images in one slab will also induce images in the other slab, etc. It follows that the total interaction in the system of charges settled in between conductor slabs can be divided into three terms: the direct charge-charge interaction as if there are no slabs, the charge-image interaction as if only one slab is present, and the image-image interaction involved by the presence of both slabs.

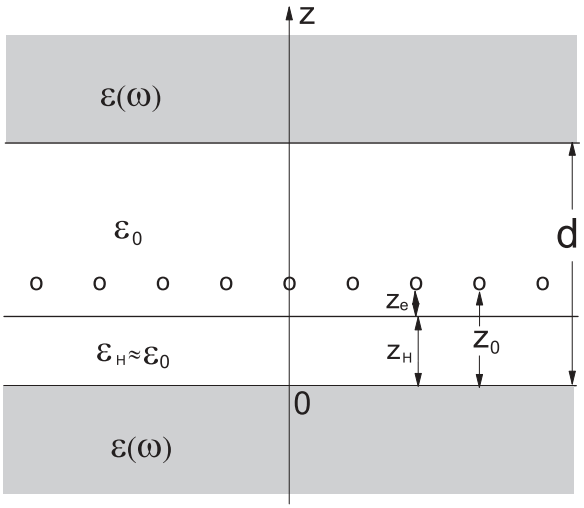

FIG. 1. Geometry of the system.

From the *quantum-mechanical* point of view, it follows that, even if we remove the Wigner lattice, neutral slabs will interact due to the fluctuation of the electromagnetic field (the Casimir effect [1]). With the presence of the Wigner lattice, the field is obviously changed and one wants to know how the interaction between the slabs looks in the new configuration.

To answer this question, we start from the quantum electrodynamics approach, i.e., we describe the dielectric properties of involved media by the appropriate dielectric functions and calculate their interaction with the electromagnetic field (including the lattice electrons) through the coupled collective modes. We shall make some approximations that will make our calculation easier and much more transparent so that we can clearly understand the role of each term in the total Hamiltonian of the system. We expect that our model can handle simultaneously the Casimir and the image potential contribution to the force between the dielectric or metallic slabs since they come from the same electromagnetic field. Finally, we want to determine which contribution is dominant with respect to various parameters that characterize the system.

The article is organized as follows. In Sec. II we analyze the Hamiltonian of our system and quantize it in terms of Wigner phonons and polariton field operators in the coherent state. In Sec. III we calculate all relevant terms needed to define the interaction between the electron lattice and the external slabs (image potential). The total force on the lattice electrons as well as the total force on the external slabs (i.e., the image and the Casimir force) are calculated and discussed in Sec. IV. The conclusion is given in Sec. V.

II. MODEL HAMILTONIAN

We discuss the system consisting of an electron (Wigner) lattice configured on z_H thick liquid He layer settled in between two semi-infinite dielectric slabs at a distance d (Fig. 1).

The total Hamiltonian of the system is given as

$$H = H_P + H_W + H_I, \tag{1}$$

where H_P represents the Hamiltonian of the electromagnetic field in the system without the Wigner lattice, H_W is the Hamiltonian of the electron lattice, and H_I is the interaction between them.

H_P can be written in terms of the photon-polarization eigenmodes. Assuming a periodic solution in time with a frequency ω, we define the constitutive equation between an electric field $\mathbf{E}$ and an ionic polarization $\mathbf{P}$ in the dielectric slabs as

$$\mathbf{P}(\mathbf{r},\omega) = \chi(\mathbf{r},\omega)\mathbf{E}(\mathbf{r},\omega). \tag{2}$$

In the standard approach, the electromagnetic field interacts with plasma oscillations in the slabs, giving

$$\chi(\omega) = \frac{\omega_P^2}{4\pi}\frac{1}{\left[\omega_T^2 - \omega^2\right]}, \tag{3}$$

where ω_T and ω_P are transverse and plasma frequencies of ions in polar dielectric, respectively. The total dielectric constant ϵ in the slabs includes an electronic contribution ϵ_∞^e at high frequencies ($\omega \gg \omega_P$):

$$\epsilon(\omega) = \epsilon_\infty^e + 4\pi\chi(\omega). \tag{4}$$

In the case of a metallic slab we put $\omega_T = 0$, $\epsilon_\infty^e = 1$, and ω_P describes the free-electron plasma frequency.

The media in between the slabs are inert dielectrics: liquid He with $\epsilon_H = 1.057$, and a vacuum layer with $\epsilon_0 = 1$. With these assumptions we can quantize the field Hamiltonian H_P in a straightforward way [14]. Let us outline some steps important for the present article. In agreement with Eqs. (2), (3), and (4), H_P takes the form

$$H_P = \int d\mathbf{r}\left\{\frac{1}{8\pi}(\epsilon_\infty\mathbf{E}^2 + \mathbf{B}^2) + \frac{2\pi}{\omega_P^2}\left(\dot{\mathbf{P}}^2 + \omega_T^2\mathbf{P}^2\right)\right\}, \tag{5}$$

where $\epsilon_\infty \equiv \epsilon_\infty(\mathbf{r})$ stands for the high-frequency dielectric constant of each particular medium in the system. In our model we have four different regions, depicted in Fig. 1: vacuum layer ($\ell = 0$) at $z_H < z < d$, with $\epsilon_\infty = \epsilon_0$, liquid He ($\ell = 1$) at $0 < z < z_H$, with $\epsilon_\infty = \epsilon_H$, and dielectric slab at $z < 0$ ($\ell = 2$) and at $z > d$ ($\ell = 3$), with $\epsilon_\infty = \epsilon_\infty^e$.

We solve the Maxwell equations by describing the electric $\mathbf{E}$ and magnetic $\mathbf{B}$ fields in a system via the vector potential $\mathbf{A_0}$ only:

$$\mathbf{E} = -\frac{1}{c}\frac{\partial\mathbf{A}_0}{\partial t}, \quad \mathbf{B} = \nabla\times\mathbf{A}_0, \tag{6}$$

and expand $\mathbf{A_0}$ in terms of coupled photon-polarization eigenmodes (*polaritons*) $\mathbf{A}_K(\mathbf{r})$:

$$\mathbf{A_0}(\mathbf{r},t) = \frac{1}{\sqrt{V}}\sum_K \zeta_K[a_K e^{-i\omega_K t}\mathbf{A}_K(\mathbf{r}) + a_K^\dagger e^{i\omega_K t}\mathbf{A}_K^*(\mathbf{r})], \tag{7}$$

which satisfy the eigenequation

$$\nabla\times\nabla\times\mathbf{A}_K(\mathbf{r}) - \frac{1}{c^2}\epsilon_K(\mathbf{r})\omega_K^2\mathbf{A}_K(\mathbf{r}) = 0 \tag{8}$$

and the gauge requirement [14,15]

$$\nabla\cdot[\epsilon_K(\mathbf{r})\mathbf{A}_K(\mathbf{r})] = 0. \tag{9}$$

Here index K enumerates all the eigenmodes in the system with the eigenfrequencies ω_K. The expansion parameter

$$\zeta_K = \sqrt{hc^2/\omega_K N_K} \tag{10}$$

depends on the orthonormality relation through the parameter N_K, which we shall determine later.

Let us expand the polarization $\mathbf{P}(\mathbf{r},t)$ in terms of polarization eigenmodes $\mathbf{P}_K$ in the same way as the vector potential $\mathbf{A_0}$ [Eq. (7)]:

$$\mathbf{P}(\mathbf{r},t) = \frac{1}{\sqrt{V}} \sum_K \zeta_K [a_K e^{-i\omega_K t} \mathbf{P}_K(\mathbf{r}) + a_K^\dagger e^{i\omega_K t} \mathbf{P}_K^*(\mathbf{r})] \,. \tag{11}$$

Assuming that $a_K^\dagger, a_K$ are the standard creation and annihilation operators of the polariton field, we obtain the quantized form of the Hamiltonian H_P [Eq. (5)], which describes the retarded electromagnetic field interacting with the dielectric media:

$$H_P = \sum_K \hbar\omega_K \left(a_K^\dagger a_K + \frac{1}{2} \right). \tag{12}$$

The second term H_W in Eq. (1) stands for the Hamiltonian of the electron layer placed on top of the liquid He surface:

$$H_W = \frac{1}{2} \sum_j \left[\frac{1}{m_e} \left(\mathbf{p}_j - \frac{e}{c} \mathbf{A}_{0j} \right)^2 + e\phi(\mathbf{r}_j) \right]. \tag{13}$$

Here $\mathbf{r}_j$ denotes the position of electron j in the layer, with the momentum $\mathbf{p}_j$. The potential $\phi(\mathbf{r})$ is determined by the electron charge density $\rho(\mathbf{r}) = e \sum_j \delta(\mathbf{r} - \mathbf{r}_j)$ and the high-frequency dielectric constants $\epsilon_\infty(\mathbf{r})$ [14]:

$$\nabla \cdot [\epsilon_\infty(\mathbf{r}) \nabla \phi(\mathbf{r})] = -4\pi\rho(\mathbf{r}). \tag{14}$$

We shall assume that the concentration of electrons n_e on the He layer is sufficiently low, so that they form the quasi-2D Wigner lattice. Typically it requires $n_e < 10^{13}\,\mathrm{cm}^{-2}$ [9] or $r_0 \gtrsim 4$ nm, where r_0 is the parameter of the 2D hexagonal lattice, and $1/n_e = (\sqrt{3}/2)\, r_0^2$. In the model of a quasi-2D Wigner lattice, one takes into account the perpendicular delocalization of lattice electron wave function [16] that leads to the average position z_e of the Wigner lattice above the He surface (Fig. 1) and to small changes in phonon frequencies.

The vector potential $\mathbf{A}_{0j}$ in Eq. (13) is responsible for the retarded interaction of lattice electrons with the electromagnetic field. It turns out [17] that this interaction will not change phonon frequencies in the presence of a metallic slab, since typical frequencies in metals (ω_P) are much higher than Wigner frequencies [18]. Only a small change in the dispersion relation is expected in the presence of an ionic crystal, if the frequency spectrums of the Wigner and crystal phonons coincide ($\omega_L \gtrsim \omega \gtrsim \omega_T$). Therefore we can write H_W in a standard second-quantized form

$$H_W = \sum_{\mu\boldsymbol{\kappa}} \hbar\omega_{\mu\boldsymbol{\kappa}} \left(c_{\mu\boldsymbol{\kappa}}^\dagger c_{\mu\boldsymbol{\kappa}} + \frac{1}{2} \right), \tag{15}$$

where $\omega_{\mu\boldsymbol{k}}$ are phonon eigenfrequencies of lattice electrons, determined by the wave vector $\boldsymbol{\kappa}$ from the first Brillouin zone and by the longitudinal or transverse polarization μ. In this article we are not interested in specific properties of the Wigner lattice, such as the phase transition. Moreover, with the approximations for $\phi(\mathbf{r})$ described in detail in Sec. III A, it turns out that properties of Wigner phonons will not be important for our further discussion.

The last term in Eq. (1) represents the interaction between the Wigner lattice and the polarization field [14]:

$$H_I = \int d\mathbf{r}\, \mathbf{P} \cdot \nabla\phi. \tag{16}$$

Having in mind that the characteristic frequencies in polar dielectric and particularly in metallic slabs are typically much higher than the lattice frequencies, we shall calculate H_I assuming that the lattice electrons are in their equilibrium positions. In this approximation, the potential ϕ describes the interaction between electrons in their lattice sites $\boldsymbol{\rho}_j$, placed $z_0 = (z_e + z_H)$ above the dielectric slab (Fig. 1).

Let us define new operators,

$$b_K = a_K + \alpha_K e^{i\omega_K t}, \tag{17}$$

which satisfy boson commutation relations

$$[b_K, b_{K'}^\dagger] = [a_K, a_{K'}^\dagger] = \delta_{K,K'},$$

and replace a_K with b_K in expressions for $\mathbf{P}(\mathbf{r},t)$ and H_P [Eqs. (11) and (12), respectively]. With the definition

$$\alpha_K = \frac{\zeta_K}{\hbar\omega_K} \frac{1}{\sqrt{V}} \int d\mathbf{r}\, \mathbf{P}_K^*(\mathbf{r}) \cdot \nabla\phi(\mathbf{r}) \tag{18}$$

we can write the field Hamiltonian together with its interaction with the electron lattice in the diagonal form as

$$H_P + H_I = H_P^C + W_{\mathrm{im}} \,.$$

The renormalized Hamiltonian

$$H_P^C = \sum_K \hbar\omega_K \left(b_K^\dagger b_K + \frac{1}{2} \right) \tag{19}$$

represents the polariton field with the same eigenfrequencies ω_K as derived in the undisturbed Hamiltonian H_P [Eq. (12)]. We say that the polaritons are, due to the interaction with Wigner electrons, in the coherent states with energy which differs from the energy of noninteracting states by the image potential

$$W_{\mathrm{im}} = -\sum_K \hbar\omega_K |\alpha_K|^2 \,. \tag{20}$$

Obviously, H_P^C and H_P have the same ground-state energy and therefore they describe the same Casimir effect, i.e., give the same attractive force between the two dielectric or metallic slabs. The additional force between the slabs follows from the image potential W_{im}, given by Eq. (20).

III. IMAGE POTENTIAL

In order to determine the image potential W_{im}, we have to calculate the parameter α_K, i.e., the polarization eigenmodes $\mathbf{P}_K(\mathbf{r})$ with the eigenfrequencies ω_K, and the scalar potential $\phi(\mathbf{r})$.

A. Scalar potential

Following Eq. (14), the scalar potential $\phi(\mathbf{r})$ is determined by the charge density $\rho(\mathbf{r})$ of Wigner electrons that are formally surrounded with media described by dielectric constant $\epsilon_\infty(\mathbf{r})$. After transforming the scalar potential into

the two-dimensional **k** space,

$$\phi(\boldsymbol{\rho},z) = A\int d\mathbf{k}\; e^{i\mathbf{k}\boldsymbol{\rho}}\;\phi(k,z),$$

where A is the normalization area (surface of the slab), we can easily find solutions for $\phi(\mathbf{k},z)$. In the medium ℓ without charges we have a homogeneous solution:

$$\phi(k,z) = a_\ell e^{-kz} + b_\ell e^{+kz}\quad,\quad \ell = (1,2,3),$$

while in the $\ell = 0$ medium with the electron charge density $\rho(\mathbf{r}) = e\sum_j \delta(\boldsymbol{\rho}-\boldsymbol{\rho}_j)\delta(z-z_0)$ we have to add the nonhomogeneous part:

$$\phi(k,z) = a_0 e^{-kz} + b_0 e^{+kz} + \sum_j C_j e^{-k|z-z_0|}\;.$$

The summation $\sum_j$ is performed over all Wigner electrons $j = 1,2,\ldots,N$, and

$$C_j = \frac{e}{2\epsilon_0\pi k}\frac{1}{A}\exp(-i\mathbf{k}\cdot\boldsymbol{\rho}_j).$$

The coefficients (a_ℓ,b_ℓ) can be determined in a standard way from the continuity of $\phi(z)$ and $\epsilon_\infty(z)\partial\phi/\partial z$. To simplify our calculations we shall make two assumptions: (i) The influence of the He layer enters through the factor $(\epsilon_H-1)/(\epsilon_H+1) = 0.027$ [16], which is very small, so we shall put $\epsilon_H = \epsilon_0 = 1$, and (ii) for the semi-infinite slabs we shall put $\epsilon^e_\infty = 1$. This is correct for metallic slabs, which are of our main interest, but for polar dielectrics one typically finds $\epsilon^e_\infty > 1$. Neglecting this influence, we can put $\epsilon_\infty(z) = \epsilon_0$ in the whole space, which leads to the simple expressions for the scalar potential of Wigner electrons z_0 above the dielectric surface:

$$\phi(k,z) = e^{-k|z-z_0|}\sum_j C_j. \tag{21}$$

In this approximation the potential in the lattice plane takes a standard form

$$\phi(\boldsymbol{\rho},z_0) = \frac{e}{\epsilon_0}\sum_j \frac{1}{|\boldsymbol{\rho}-\boldsymbol{\rho}_j|}$$

and it does not depend upon z_0 or d.

B. Polarization

In Sec. II we introduced the retarded polarization $\mathbf{P}(\mathbf{r})$ [Eq. (11)], with eigenmodes $\mathbf{P}_K$ related to $\mathbf{A}_K$ through Eqs. (2) and (6):

$$\mathbf{P}_K(\mathbf{r}) = i\frac{\omega_K}{c}\chi_K(\mathbf{r})\mathbf{A}_K(\mathbf{r}). \tag{22}$$

The mode spectrum follows from Eqs. (4), (8), and (9). The trivial solution $\epsilon_K(\mathbf{r}) = 0$ leads to (nonretarded) volume modes in each dielectric slab, with a longitudinal plasma frequency $\omega_L = [\omega_T^2 + \omega_P^2/\epsilon_0]^{1/2}$. Since those modes do not produce the field outside the slabs we shall neglect them in further discussion. The polariton modes that give field outside the dielectric slabs are surface modes with exponentially decaying fields in the dielectrics and in the gap, guided modes which decay in the dielectrics but oscillate in the gap, and propagating modes which oscillate in the dielectrics (and in the $z\to\pm\infty$ limit). Using the planar symmetry, we can characterize each one by the wave vector **k** parallel to the dielectric surfaces, the perpendicular wave vector β_ℓ in a medium ℓ, $\beta_\ell(\omega,k) = [\epsilon_\ell\omega^2/c^2 - k^2]^{1/2}$, and the polarization index q denoting TM or TE polarization. To simplify notation, we shall denote by $s = (q,\beta_\ell)$ all polarization eigenmodes with the same wave vector **k**, so we put $K = (\mathbf{k},s)$ and write

$$\mathbf{P}_K(\mathbf{r}) = \mathbf{P}_{\mathbf{k}s}(z)e^{i\mathbf{k}\cdot\boldsymbol{\rho}}\;. \tag{23}$$

All modes, surface, guided, and propagating ones, interact with point charges in the Wigner lattice, giving the image potential $W_{\rm im}$ [Eq. (20)], equal to the one derived in the nonretarded limit [19]. In the nonretarded limit, however, only surface modes interact with the Wigner lattice, making the calculation of $W_{\rm im}$ much simpler.

The nonretarded polarization $\mathbf{P}(\mathbf{r},t)$ is formally expanded in the same way as the retarded one given by Eq. (11) [14]. Choosing the parameter $N_K = (4\pi c)^2$ gives for the expansion parameter $\zeta_K = (1/4\pi)\sqrt{h/\omega_K}$, and the orthonormality relation for the eigenmodes $\mathbf{P}_K$ becomes

$$\frac{1}{V}\int d\mathbf{r}\frac{1}{\omega_P^2(\mathbf{r})}\mathbf{P}^*_K(\mathbf{r})\cdot\mathbf{P}_{K'}(\mathbf{r}) = \delta_{K,K'}. \tag{24}$$

The nonretarded polarization eigenmodes (*plasmons*) can be put in the form

$$\mathbf{P}_K(\mathbf{r}) = -\chi_K(\mathbf{r})\nabla\Phi_K(\mathbf{r}), \tag{25}$$

where the "polarization" potential $\Phi_K(\mathbf{r})$ satisfies

$$\nabla[\epsilon_K(\mathbf{r})\nabla\Phi_K(\mathbf{r})] = 0.$$

Since we are not interested in volume modes, determined by $\epsilon_K(\mathbf{r}) = 0$, we are left with the surface plasmons satisfying in each medium ℓ the relation

$$\Delta\Phi_K(\mathbf{r}) = 0,\quad \ell = (0,1,2,3). \tag{26}$$

Using the planar symmetry we can put $K = (\mathbf{k},\sigma)$ in Eq. (23), where σ enumerates all (nonretarded) surface modes. From Eq. (25) we find the polarization in each medium ℓ:

$$\mathbf{P}_{\mathbf{k}\sigma}(z) = -\chi_{k\sigma}(z)k\left(i\hat{\mathbf{k}} + \hat{\mathbf{z}}\frac{1}{k}\frac{\partial}{\partial z}\right)\Phi_{k\sigma}(z), \tag{27}$$

where the potential $\Phi_{k\sigma}(z)$ follows from Eq. (26):

$$\Phi_{k\sigma}(z) = f_\ell e^{-kz} + g_\ell e^{+kz},\quad \ell = (0,1,2,3). \tag{28}$$

The coefficients (f_ℓ,g_ℓ) follow in a standard way from the continuity of $\Phi_{k\sigma}(z)$ and $\epsilon_{k\sigma}(z)\frac{\partial}{\partial z}\Phi_{k\sigma}(z)$. The requirement for the nontrivial solutions of the coefficients leads to the dispersion relation of two surface plasmon modes ($\sigma = +,-$) that exist in the semi-infinite dielectric plates with the gap in between. With our assumption $\epsilon_\infty(z) = \epsilon_0$ we can write the dispersion relation of the plasmon eigenfrequencies in the explicit form

$$\omega^2_\pm(k) = \omega_a^2 \pm \tfrac{1}{2}\left(\omega_L^2 - \omega_T^2\right)e^{-kd}\;. \tag{29}$$

The asymptotic ($k\to\infty$) frequency

$$\omega_a^2 \equiv \omega^2_\pm(k\to\infty) = \tfrac{1}{2}\left(\omega_L^2 + \omega_T^2\right)$$

represents also the frequency of the (nondispersive) plasmon mode in the case where the plates are completely separated ($d\to\infty$) or only one plate is present ($d = \infty$).

Inside the dielectrics we find "polarization" potential [Eq. (28)], corresponding to $\omega_{\pm}(k)$ modes:

$$\Phi_{k\pm}(z) = \gamma_{\pm}(k) \begin{cases} e^{kz} & : \quad z < 0 \\ \pm e^{-k(z-d)} & : \quad z > d. \end{cases} \tag{30}$$

Since $\mathbf{P}_{\mathbf{k}\sigma}(z) = 0$ outside the dielectric slabs, Eqs. (27) and (30) determine the polarization in our system. With the help of the orthonormality relation [Eq. (24)], we find the normalization factor

$$\gamma_{\pm}^2(k) = L \frac{1}{2k} \frac{\omega_P^2}{\chi^2(\omega_{\pm}(k))},$$

where L is the normalization length, i.e., the thickness of dielectric slabs.

C. Image potential

The image potential W_{im} [Eq. (20)] is determined by the "shift parameter" $\alpha_{\mathbf{k}\sigma}$, given by Eq. (18). The integration in Eq. (18) extends only over the dielectric slabs, and from Eqs. (2) and (9) we find $\nabla \mathbf{P} = 0$ inside the slabs. Therefore the integrand in Eq. (18) can be transformed into $\nabla(\mathbf{P}\phi)$, and the integration over the slabs replaced with the values of the integrand at the surfaces of the slabs $z = 0$ and $z = d$:

$$\alpha_{\mathbf{k}\sigma} = \frac{\zeta_{k\sigma}}{\hbar\omega_{\sigma}(k)} \frac{A}{\sqrt{V}} (2\pi)^2 \left[\hat{\mathbf{z}} \cdot \mathbf{P}^*_{\mathbf{k}\sigma}(z)\phi(k,z)\right]_{z=0}^{z=d}.$$

Inserting the corresponding boundary values in $\mathbf{P}_{\mathbf{k}\sigma}(z)$ [Eq. (27)] and $\phi(k,z)$ [Eq. (21)], the image potential takes form

$$W_{\text{im}} = -\frac{e^2}{16\pi\epsilon_0}\left(\omega_L^2 - \omega_T^2\right) \sum_{\sigma=+,-} \int_0^{\infty} \frac{dk}{\omega_{\sigma}^2(k)} \int_0^{2\pi} d\phi |S_{\sigma}(\mathbf{k})|^2$$

with

$$S_{\pm}(\mathbf{k}) = [e^{-kz_0} \pm e^{-k(d-z_0)}] \sum_j e^{-i\mathbf{k}\boldsymbol{\rho}_j}.$$

If there is only one electron at $\boldsymbol{\rho}_j = 0$ interacting with metallic plates, we can easily recover results for the image potential derived in Ref. [20]. In the case of Wigner lattice we have to sum up over N lattice electrons, which leads to

$$W_{\text{im}} = -N \frac{e^2}{2\epsilon_0} \Omega \sum_j F_j, \tag{31}$$

$$F_j = \int_0^{\infty} dk J_0(k\rho_j) \frac{e^{-2kz_0} + e^{-2k(d-z_0)} - 2\Omega e^{-2kd}}{1 - \Omega^2 e^{-2kd}}, \tag{32}$$

where J_0 is the Bessel function. With the explicit form of the dispersion relation [Eq. (29)], it turns out that the dielectric properties of the slabs are described only by the factor

$$\Omega = \left(\omega_L^2 - \omega_T^2\right)/\left(\omega_L^2 + \omega_T^2\right). \tag{33}$$

The expansion of the denominator in Eq. (32) gives the interaction of an electron with the dielectric plates in terms of a series of images. The expansion converges for $\Omega < 1$, but in the limit $\Omega = 1$ at the $k = 0$ convergence problems may appear. Therefore we shall retain Ω in all our expansions and for the metallic plates (with $\omega_T = 0$) we shall simply put $\Omega = 1$ in the final result.

After expanding the denominator and integrating over k we find

$$F_j = \frac{1}{\sqrt{\rho_j^2 + 4z_0^2}} + \sum_{n=1}^{\infty} \Omega^{2(n-1)} S_j^n,$$

where

$$S_j^n = \frac{\Omega^2}{\sqrt{\rho_j^2 + 4(nd + z_0)^2}} + \frac{1}{\sqrt{\rho_j^2 + 4(nd - z_0)^2}} - \frac{2\Omega}{\sqrt{\rho_j^2 + 4(nd)^2}}.$$

The infinite number of images ($n = 1,2,3...$) of each electron has to be summed up for all electrons ($j = 1,2,3...$) in the lattice. In order to perform summations efficiently, we shall first take the x transformation $[1/\sqrt{a} = (2/\sqrt{\pi}) \int_0^{\infty} \exp(-ax^2)]$ and rewrite F_j as

$$F_j = \frac{2}{\sqrt{\pi}} \int_0^{\infty} dx e^{-\rho_j^2 x^2} f_d(x). \tag{34}$$

Now we shall divide the contribution to the image potential, described by $f_d(x)$, into two parts

$$f_d(x) = f_d^{\infty}(x) + \Delta f_d(x), \tag{35}$$

$$f_d^{\infty}(x) = e^{-4z_0^2 x^2} + e^{-4(d-z_0)^2 x^2}, \tag{36}$$

$$\Delta f_d(x) = \sum_{n=1}^{\infty} \Omega^{2n} \left[e^{-4(nd+z_0)^2 x^2} + e^{-4((n+1)d-z_0)^2 x^2} - \frac{2}{\Omega} e^{-4(nd)^2 x^2} \right]. \tag{37}$$

The first part $f_d^{\infty}(x)$ in Eq. (35) describes the "direct images" of Wigner electrons that exist in each dielectric slab regardless of the other slab. Therefore, if we completely separate the plates ($d \to \infty$) and take a distance between the lattice electrons and one plate [z_0 or $(d - z_0)$] as fixed, $f_d^{\infty}(x)$ will describe completely the interaction of this plate with the Wigner lattice. In that sense the second part $\Delta f_d(x)$ represents the interaction between the plates (image-image interaction) and it vanishes in the $d \to \infty$ limit.

The form of $f_d(x)$ enables us to perform the summation over all lattice electrons using the Ewald transformation,

$$\sum_j e^{-\rho_j^2 x^2} = \frac{1}{S_0} \frac{\pi}{x^2} \sum_{\mathbf{G}} e^{-G^2/4x^2},$$

where the summation over direct lattice sites $\boldsymbol{\rho}_j$ is replaced by the summation over reciprocal lattice sites $\mathbf{G}$. $S_0 = A/N = 1/n_e$ is the average area per electron. In applying the Ewald transformation one introduces a critical parameter η so that the slow-converging terms with $x < \eta$ in the direct space are replaced by the fast-converging terms in the

reciprocal space:

$$\sum_j F_j = \frac{2}{\sqrt{\pi}}\left[\frac{\pi}{S_0}\sum_{\mathbf{G}}\int_0^{\eta}\frac{dx}{x^2}e^{-G^2/4x^2}f_d(x) + \sum_j\int_{\eta}^{\infty}dx e^{-\rho_j^2x^2}f_d(x)\right]. \quad (38)$$

In Eq. (38) there are two specific terms of particular interest: $j=0$, i.e., $\boldsymbol{\rho}=0$, and $\mathbf{G}=0$, which we shall calculate separately. Introducing the extended Misra functions [16]

$$\Phi_n^R(y) = \int_1^{\infty} dt\, t^n\, e^{-yt} f_d(\eta\sqrt{t}),$$

$$\Phi_n^G(y) = \int_1^{\infty} dt\, t^n\, e^{-yt} f_d(\eta/\sqrt{t}),$$

we find

$$\sum_j F_j = F_d(\boldsymbol{\rho}=0) + F_d(\mathbf{G}=0) + a_\eta\left[\sum_{\mathbf{G}\neq 0}\Phi^G_{-1/2}\left(\frac{G^2}{4\eta^2}\right) - \Phi^R_{-3/2}(0)\right] + b_\eta\left[\sum_{j\neq 0}\Phi^R_{-1/2}\left(\eta^2\rho_j^2\right) - \Phi^G_{-3/2}(0)\right], \quad (39)$$

with the expansion coefficients equal to $a_\eta = (1/\eta)(g_0/2\sqrt{\pi}r_0)$, $b_\eta = \eta/\sqrt{\pi}$, and g_0 being the reciprocal lattice parameter that satisfies $S_0 = 2\pi r_0/g_0$.

To obtain the $\boldsymbol{\rho}=0$ term of Eq. (38), i.e., the interaction $F_d(\boldsymbol{\rho}=0)$ of a single electron with the dielectric slabs, we shall divide it according to Eq. (35) in two terms:

$$F_d(\boldsymbol{\rho}=0) = \frac{2}{\pi}\int_0^{\infty} dx f_d(x) = F_d^{\infty}(\boldsymbol{\rho}=0) + \Delta F_d(\boldsymbol{\rho}=0).$$

The first term involves f_d^{∞} and it gives a direct interaction of a single electron with both dielectric plates:

$$F_d^{\infty}(\boldsymbol{\rho}=0) = \frac{1}{2}\left[\frac{1}{z_0} + \frac{1}{d-z_0}\right].$$

The second term involves Δf_d and it represents a slow-converging ($\sim\frac{1}{n}$) image-image interaction. However, one can calculate explicitly the contribution at $z_0 = d/2$ and expand the rest of the sum in terms of $z_c = 1 - 2z_0/d$ that converges much faster ($\sim\frac{1}{n^3}$):

$$\Delta F_d(\boldsymbol{\rho}=0) = -\frac{2}{d}\left[1 - \frac{\ln(1+\Omega)}{\Omega} - z_c^2\sum_{n=1}^{\infty}\Omega^{2n}\frac{1}{(2n+1)\left[(2n+1)^2 - z_c^2\right]}\right].$$

Note that in the middle of the gap ($z_c = 0$) we find $F_d(\boldsymbol{\rho}=0) = (2/d)\ln(1+\Omega)/\Omega$, in agreement with Ref. [20].

The $\mathbf{G}=0$ term is connected with the image potential [Eq. (31)], averaged over all lattice sites:

$$\frac{1}{N}\langle W_{\rm im}\rangle \equiv \frac{1}{A}\int d\boldsymbol{\rho}\, W_{\rm im}(\boldsymbol{\rho}) = -\frac{\Omega}{2}\frac{e^2}{\epsilon_0}F_d(\mathbf{G}=0). \quad (40)$$

Following again Eq. (35), the $F_d(\mathbf{G}=0)$ term can be divided as

$$F_d(\mathbf{G}=0) = \frac{2\sqrt{\pi}}{S_0}\int_0^{\infty}\frac{dx}{x^2}f_d(x) = F_d^{\infty}(\mathbf{G}=0) + \Delta F_d(\mathbf{G}=0). \quad (41)$$

Both terms of $F_d(\mathbf{G}=0)$ diverge, and we shall discuss its divergence in more detail in the next section. Since $\langle W_{\rm im}\rangle$ diverges, one can eventually subtract $\langle W_{\rm im}\rangle$ (i.e., the $\mathbf{k}=0$ component) when calculating the image potential via Eqs. (31) and (39).

All the extended Misra functions in Eq. (39) are finite, so by choosing $\eta = (g_0/2r_0)^{1/2}$ [16], the summation over the reciprocal ($\mathbf{G}\neq 0$) and direct ($j\neq 0$) lattice sites converges equally fast.

IV. RESULTS AND DISCUSSION

Let us briefly summarize our results. The total ground-state energy of the Hamiltonian of the system, given by Eq. (1), can be written as

$$E_{\rm tot} = E_P + E_W + E_I, \quad (42)$$

where E_P is the ground-state energy of the polariton field, E_W the energy of the Wigner lattice, and E_I energy due to the interaction of the Wigner lattice with the dielectric slabs.

According to the Hamiltonian of the polariton field H_P^C [Eq. (19)] or equivalently, H_P [Eq. (12)], E_P takes the form

$$E_P = \frac{1}{2}\sum_{\mathbf{k}s}\hbar\omega_{\mathbf{k}s},$$

which diverges at large k values. Therefore one calculates the Casimir energy E_C instead, i.e., the difference between the ground-state energy of the electromagnetic field in the system with the dielectric slabs and in the free space [21]. In our model, with the appropriate regulation, we take a simple expression for the Casimir energy [22–24],

$$E_C = \frac{\hbar A}{4\pi^2c^2}\int_1^{\infty}dpp\int_0^{\infty}d\xi\xi^2\sum_q\ln[1 - Q^q(i\xi,p)], \quad (43)$$

where the summation over the polariton modes with polarization q is replaced by the integration over the imaginary frequency $\xi = -i\omega$ of the nonpropagating modes, and over the parameter p defined with $k^2 = (\xi^2/c^2)(p^2-1)$. The eigenfrequencies of nonpropagating modes (surface and guided modes, with disappearing field in the $z\to\pm\infty$ limit) are determined by the dispersion relation [24]

$$Q^q(\omega,k) \equiv [r^q(\omega,k)]^2\, e^{-2\alpha_0 d} = 1,$$

where $r^q(\omega,k)$ are Fresnel reflection coefficients at the vacuum-dielectric interface, and $\alpha_0 \equiv -i\beta_0(\omega,k) = (\xi/c)\sqrt{p^2-1+\epsilon_0}$.

The interaction H_I [Eq. (16)] between the Wigner lattice and the dielectric plates leads to the image potential with the energy $E_I = W_{\rm im}$ [Eq. (31)].

The Hamiltonian of the Wigner lattice H_W [Eq. (13)] is calculated in our model with the electrons in their average perpendicular positions z_0 to obtain Eq. (15). In this approximation, the direct interaction between the Wigner electrons is

independent of z_0 and d, so here we assume that E_W depends only upon the charge density of lattice electrons.

Knowing all the energy terms in Eq. (42), we shall now calculate corresponding forces that will not depend upon the renormalization constants eventually involved in some energy terms.

A. Image force on Wigner lattice

Let us first analyze the total (perpendicular) force $\mathcal{F}_{\rm tot}^{z_0}$ acting on an electron in the Wigner lattice. Since only $W_{\rm im}$ depends on z_0, we find

$$\mathcal{F}_{\rm tot}^{z_0} \equiv -\frac{1}{N}\frac{\partial}{\partial z_0}E_{\rm tot} = -\frac{e^2}{2\epsilon_0}\Omega\frac{\partial}{\partial z_0}\sum_j F_j. \qquad (44)$$

The calculation of $\frac{\partial}{\partial z_0}\sum_j F_j$ requires the evaluation of terms of Eq. (39). The first term determines the image force on a single charge located at $(\boldsymbol{\rho}=0,z_0)$ in between the slabs,

$$\mathcal{F}_1^{z_0} = -\frac{e^2}{2\epsilon_0}\Omega\frac{\partial}{\partial z_0}F_d(\boldsymbol{\rho}=0). \qquad (45)$$

The term $F_d(\boldsymbol{\rho}=0)$ is discussed in detail in the previous section, and we can easily calculate $\mathcal{F}_1^{z_0}$.

The second, $F_d(\mathbf{G}=0)$ term, describes the average image potential $\langle W_{\rm im}\rangle$, which is divergent. However, for finite values of d we find that $\frac{\partial}{\partial z_0}F_d(\mathbf{G}=0)=0$. This is the consequence of perfect screening on both slabs, so there is no force on the average charge distribution in between the slabs. In the case when only one (lower) slab is present, the images in that slab are not screened and it follows that

$$\frac{\partial}{\partial z_0}F_d(\mathbf{G}=0) = -\frac{4\pi}{S_0}\ ,\ \ d=\infty, \qquad (46)$$

which gives a constant attractive contribution to the force between the Wigner electrons and the dielectric slab.

The rest of the terms in Eq. (39) contain extended Misra functions, and their derivatives with respect to z_0 can be easily derived and calculated.

In Fig. 2 we compare the force $\mathcal{F}_{\rm tot}^{z_0}$ [Eq. (44)] acting on the lattice electron, with the force $\mathcal{F}_1^{z_0}$ [Eq. (45)] acting on the single electron (with no lattice). The forces are normalized to $\mathcal{F}_e = e^2/2a_0^2$, where a_0 is the Bohr radius. The curves are shown for two z_0 values, satisfying $z_0 < r_0$. The forces $\mathcal{F}_{\rm tot}^{z_0}$ and $\mathcal{F}_1^{z_0}$ tend to zero when $d \to 2z_0$, and become strongly repulsive for $d < 2z_0$. In the latter case the electrons are attracted by the upper plate, which would eventually destroy the lattice. In order for the image force to stabilize the electron lattice on the liquid He layer, we should take $z_0 < d/2$. In that case the force $\mathcal{F}_1^{z_0}$ is always attractive, while the force describing the charge interaction with all other but its own images $\mathcal{F}_{\rm ind}^{z_0} = \mathcal{F}_{\rm tot}^{z_0} - \mathcal{F}_1^{z_0}$ [determined by the Misra functions Φ in Eq. (39)] is repulsive. This "indirect" screening is not significant for $z_0 \ll r_0$, but when z_0 becomes comparable with the average distance among the lattice electrons, the "indirect" screening efficiently cancels the "direct" one. At $z_0 \gg r_0$ this cancellation is complete and the lattice behaves as a continuous charge distribution, satisfying $\mathcal{F}_{\rm tot}^{z_0} \approx 0$. Note that all metallic slabs are described with $\Omega = 1$, regardless of the specific electron plasma frequency ω_P, i.e., they are all represented by the same curves.

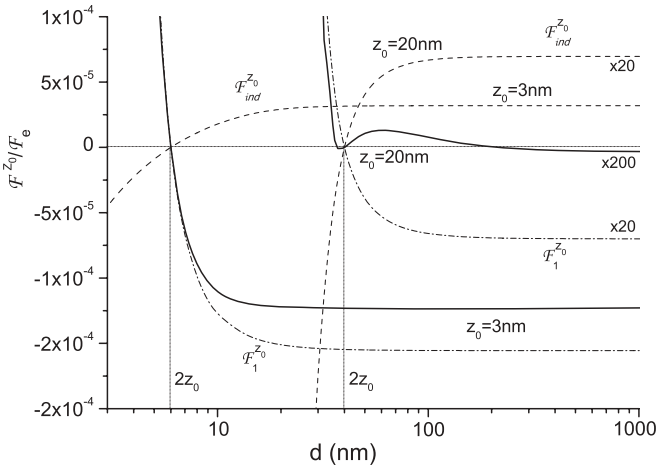

FIG. 2. The forces on the Wigner lattice as a function of the slab separation d: $\mathcal{F}_{\rm tot}^{z_0}$ (full), $\mathcal{F}_1^{z_0}$ (dash-dotted), and $\mathcal{F}_{\rm ind}^{z_0}$ (dashed) line. At $z_0 = 3$ nm, $\mathcal{F}_1^{z_0}$ dominates over $\mathcal{F}_{\rm ind}^{z_0}$, but at $z_0 = 20$ nm, we find $\mathcal{F}_{\rm ind}^{z_0} \approx -\mathcal{F}_1^{z_0}$; so the curves are enlarged in order to be presented on the same scale. The lattice parameter is $r_0 = 30$ nm.

The comparison between the forces $\mathcal{F}_{\rm tot}^{z_0}$ and $\mathcal{F}_1^{z_0}$ in the limit $z_0 \ll r_0$ is shown in Fig. 3 for different slab separations d. For all values of d when $r_0 > 10z_0$ we can neglect the influence of electron density and simply put $\mathcal{F}_{\rm tot}^{z_0} \approx \mathcal{F}_1^{z_0}$. As seen in Fig. 3, after approximately $d > 10z_0$, the forces become almost independent of d, and for all electron densities approaching to their $d \to \infty$ limit. Evidently, for the lattice located in the middle of the gap ($z_0 = d/2$) there is no force on the lattice electrons, while the total force $\mathcal{F}_{\rm tot}^{z_0}$ at low electron densities ($r_0 \gg z_0$) becomes attractive (repulsive) at $z_0 < d/2$ ($z_0 > d/2$), respectively. As pointed out, at high electron densities ($r_0 \lesssim z_0$), the "indirect" screening $\mathcal{F}_{\rm ind}^{z_0}$ becomes important, and it even overcompensates the "direct" screening $\mathcal{F}_1^{z_0}$, so that the total force $\mathcal{F}_{\rm tot}^{z_0}$ changes its sign.

The difference between the image forces in the case of metallic and dielectric slabs is shown in Fig. 4.

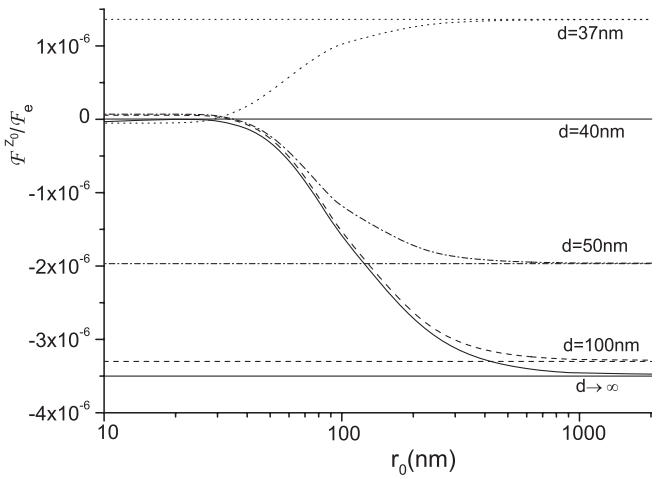

FIG. 3. The forces $\mathcal{F}_{\rm tot}^{z_0}$ and $\mathcal{F}_1^{z_0}$ on the Wigner lattice as a function of lattice parameter r_0. Results are shown for several values of d. The position of the lattice is $z_0 = 20$ nm. $\mathcal{F}_1^{z_0}$ is independent of r_0 and appears as a straight line for any value of d, while $\mathcal{F}_{\rm tot}^{z_0}$ reduces to $\mathcal{F}_1^{z_0}$ at low electron densities ($r_0 \gg z_0$).

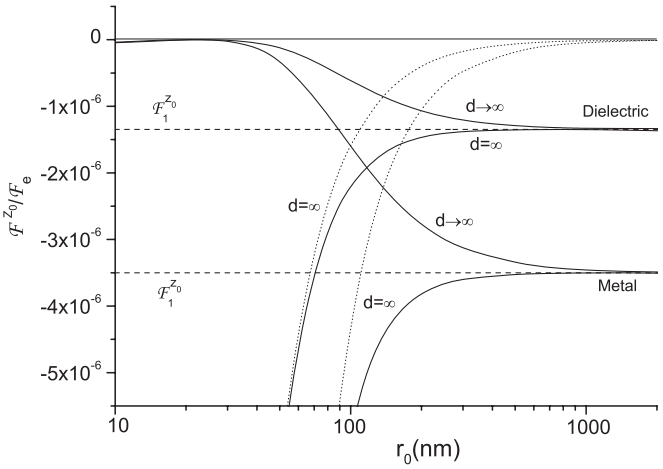

FIG. 4. The forces $\mathcal{F}_{\rm tot}^{z_0}$ (full line) and $\mathcal{F}_1^{z_0}$ (dashed line) on the Wigner lattice surrounded by the well-separated metallic or dielectric slabs ($d \to \infty$). The $\mathbf{G} = 0$ component (dotted line) contributes only if there is no upper plate ($d = \infty$). The lattice position is $z_0 = 20$ nm. For a dielectric slab we took $\omega_T = 0.02$ eV, $\omega_L = 0.03$ eV, i.e., $\Omega = 0.38$, appropriate for NaCl.

The results are given for $d \to \infty$ [i.e., $d \gg (r_0, z_0)$] and for $d = \infty$ (when there is no upper slab). As seen in the figure, the metallic slabs are more efficient in screening than the dielectric slabs, typically by a factor Ω [Eq. (33)]. As expected, at low electron densities ($r_0 \gg z_0$), the total force $\mathcal{F}_{\rm tot}^{z_0}$ is in all cases mainly determined by the force on a single electron $\mathcal{F}_1^{z_0}$, and at higher electron densities, if both slabs are present, the total force is well screened. However, if we remove the upper slab, the $\mathbf{G} = 0$ component becomes active and particularly important at higher electron densities, so $\mathcal{F}_{\rm tot}^{z_0}$ strongly attracts the electron lattice for $r_0 \lesssim z_0$. In that case the $d \to \infty$ limit (two slabs are separated at very long distance) and the $d = \infty$ case (there is only one slab in the system) represent two significantly different physical situations.

B. Total force between slabs

In this article we are particularly interested in the total force (per unit area) $\mathcal{F}_{\rm tot}^d$ acting between dielectric or metallic slabs. According to our discussion, it contains two contributions:

$$\mathcal{F}_{\rm tot}^d \equiv -\frac{1}{A}\frac{\partial}{\partial d}E_{\rm tot} = \mathcal{F}_C + \mathcal{F}_{\rm im}^d \,. \tag{47}$$

a. Casimir force $\mathcal{F}_C$. The Casimir force (per unit area) that attracts two neutral dielectric slabs at distance d due to fluctuation of the electromagnetic field can be derived directly from Eq. (43):

$$\mathcal{F}_C = -\frac{\hbar}{2\pi^2 c^2}\int_1^\infty dp\, p \int_0^\infty d\xi\, \xi^2 \alpha_0 \sum_q \frac{Q^q(i\xi,p)}{1 - Q^q(i\xi,p)}. \tag{48}$$

In the case of perfect screening [$\epsilon(\omega) = -\infty$] we find the well-known result

$$\mathcal{F}_C^0 = -\frac{\hbar c \pi^2}{240}\frac{1}{d^4}. \tag{49}$$

In real metals the Casimir force [Eq. (48)] behaves also as $\sim 1/d^4$ at large d values, but for thin slab separations it changes its behavior to $\sim 1/d^3$ [25].

b. Image force $\mathcal{F}_{\rm im}^d$. Assuming a fixed distance z_0 between the Wigner lattice and the lower dielectric slab, and using Eq. (31), we can write the image force (per unit area) acting between the dielectric slabs as

$$\mathcal{F}_{\rm im}^d = -\frac{e^2}{2\epsilon_0}\frac{\Omega}{S_0}\frac{\partial}{\partial d}\sum_j F_j = \mathcal{F}_{\rm im}^\infty + \Delta\mathcal{F}_{\rm im}^d, \tag{50}$$

where, following Eqs. (34) and (35), we have divided it into the "direct-image" $\mathcal{F}_{\rm im}^\infty$ and "image-image" $\Delta\mathcal{F}_{\rm im}^d$ part. Again, we can easily take derivatives with respect to d of each term in Eq. (50), except of the $\mathbf{G} = 0$ term. Fortunately, in that case the summation over all images can be performed analytically, and from Eq. (41) we find for a finite distance d between the slabs,

$$\frac{\partial}{\partial d}F_d^\infty(\mathbf{G} = 0) = -\frac{4\pi}{S_0}\,, \tag{51}$$

$$\frac{\partial}{\partial d}\Delta F_d(\mathbf{G} = 0) = \frac{4\pi}{S_0}\left[1 - \frac{1}{(1+\Omega)^2}\right]. \tag{52}$$

As expected, in the averaged interaction the "direct-image" term, Eq. (51), attracts the dielectric slabs, while the "image-image" term, Eq. (52), repels them. When summed together, we find that the attractive interaction prevails. The image force (per unit area) averaged over all lattice sites follows from Eq. (40):

$$\langle \mathcal{F}_{\rm im}^d \rangle = -\frac{1}{A}\frac{\partial}{\partial d}\langle W_{\rm im}\rangle = -\frac{\Omega}{2}\frac{e^2}{\epsilon_0}\frac{4\pi}{S_0^2}\frac{1}{(1+\Omega)^2}. \tag{53}$$

If we assume that only one slab is present ($d = \infty$), we would obtain the average image force to be zero: $< \mathcal{F}_{\rm im}^d > \sim \frac{\partial}{\partial d}F_d(\mathbf{G} = 0) = 0$. Note that this case is quite the opposite to the case in Sec. A, when we take the derivative with respect to z_0 [Eq. (46)].

The comparison between the Casimir and the image force acting between the metallic slabs is shown in Fig. 5. The forces are given with the negative sign in order to show them on a log scale.

At large separations between the slabs ($d > r_0$) the image force $\mathcal{F}_{\rm im}^d$ is mainly determined by the $\mathbf{G} = 0$ term and is therefore well approximated by the average image force [Eq. (53)], which is independent of d. The influence of the lattice geometry becomes important at lower slab separations ($d < r_0$) and it depends significantly on the position of the lattice z_0. We have shown data only for $d > 2z_0$, where the lattice should be stable.

According to results derived for $\mathcal{F}_{\rm im}^d$, in the system with $d < r_0$ one could get more insight into the effect of lattice geometry by measuring the force acting in between the slabs. But that is the situation when one has to take into account the Casimir force $\mathcal{F}_C$ too, as it starts to dominate in that region. Note that although the Casimir force $\mathcal{F}_C$ [Eq. (48)] depends explicitly on ω_P, this dependence is not crucial for our discussion. It can be seen from Fig. 5, where we presented the result for $\mathcal{F}_C$ with $\omega_P = 10$ eV, a typical value for real metal, and compared

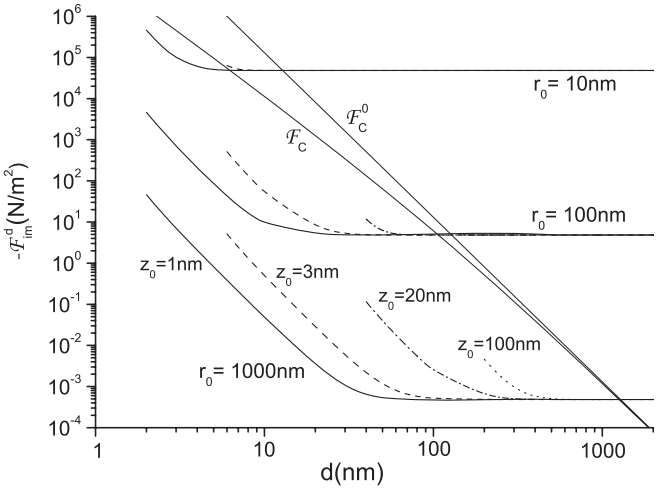

FIG. 5. Image force $\mathcal{F}^d_{\rm im}$ (in units N/m^2) as a function of metallic slab separation d. The force is shown for three different lattice parameters r_0, together with various lattice positions z_0: 1 nm (full), 3 nm (dashed), 20 nm (dash-dotted), and 100 nm (dotted) line. The Casimir forces for real ($\mathcal{F}_C$) and ideal ($\mathcal{F}^0_C$) metal are shown for comparison.

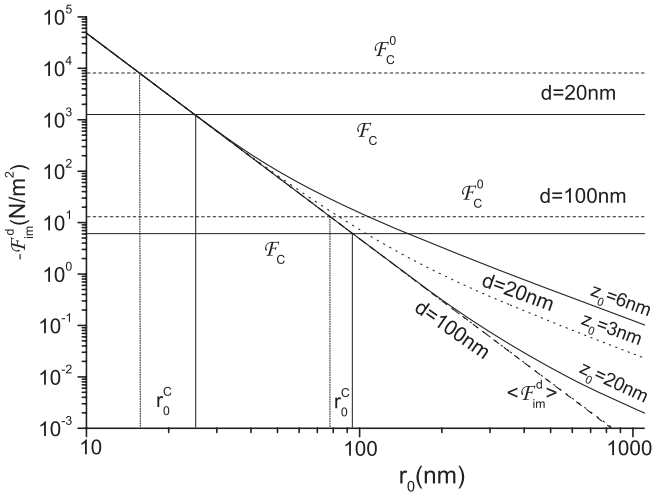

FIG. 7. Image force $\mathcal{F}^d_{\rm im}$ on metallic slabs as a function of lattice parameter r_0. Full line: ($d = 20$ nm, $z_0 = 6$ nm) and ($d = 100$ nm, $z_0 = 20$ nm). Dotted line describes the same d values, with $z_0 = 3$ nm. The averaged image potential $\langle \mathcal{F}^d_{\rm im} \rangle$ (dashed line) depends only on r_0. The Casimir forces for real ($\mathcal{F}_C$, full line) and for ideal ($\mathcal{F}^0_C$, dashed line) metallic slabs are shown for comparison.

this force with the force $\mathcal{F}^0_C$ for ideal metal [Eq. (49)] (with $\omega_P \to \infty$).

The total force $\mathcal{F}^d_{\rm tot} = \mathcal{F}^d_{\rm im} + \mathcal{F}_C$ is shown in Fig. 6 for all formally possible slab separations d allowed by the lattice position $z_0 = 20$ nm. Notice that (i) in the $d \to z_0$ limit, the lattice electrons approach the upper slab and the contribution from the image force $\mathcal{F}^d_{\rm im}$ diverges; (ii) at very high electron densities ($r_0 \lesssim 10$ nm) the contribution from the $\mathbf{G} = 0$ term does not cross the $\mathcal{F}^0_C$ curve because the crossing point requires $d < z_0$.

Let us notice that in the case of dielectric slabs, the situation is similar to that shown in Figs. 5 and in 6, except that all relevant forces are approximately an order of magnitude weaker.

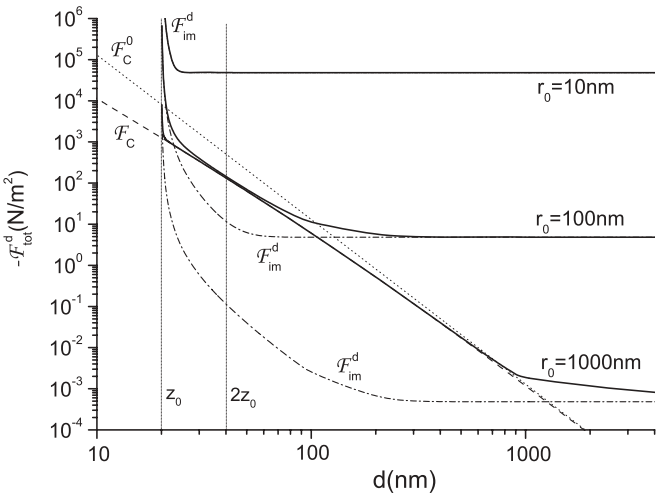

FIG. 6. Total force $\mathcal{F}^d_{\rm tot}$ (full line) on metallic slabs for different lattice parameters r_0. The contributions $\mathcal{F}^d_{\rm im}$ (dash-dotted line) and $\mathcal{F}_C$ (dashed line) to $\mathcal{F}^d_{\rm tot}$ are also shown, as well as $\mathcal{F}^0_C$ (dotted line).

Since in the whole region where the lattice could be stable ($d > 2z_0$) dominates either the $\mathbf{G} = \mathbf{0}$ term or the Casimir force, the position of the lattice z_0 has negligible influence on $\mathcal{F}^d_{\rm tot}$. In the case of metallic slabs we can roughly approximate the Casimir force by $\mathcal{F}^0_C$ [Eq. (49)], and assuming $d \gtrsim r_0$ the image force by $\langle \mathcal{F}^d_{\rm im} \rangle$ [Eq. (53)]. That enables us to easily determine the critical values d^c (for given r_0) or r^c_0 (for given d) at which those two forces are equal:

$$d^c \approx \sqrt[4]{\frac{\pi}{160}\frac{\hbar c}{e^2}}\, r_0 \;=\; 1.28\, r_0, \quad r^c_0 \;\approx\; 0.78\, d. \tag{54}$$

The critical values [Eq. (54)] that follow from $\langle \mathcal{F}^d_{\rm im} \rangle = \mathcal{F}^0_C$ are compared in Fig. 7 with the critical values that follow from $\mathcal{F}^d_{\rm im} = \mathcal{F}_C$. It comes out that r^c_0 values determined in such a way are somewhat greater compared to the values from Eq. (54), but they still do not depend on z_0, providing that the requirement $d > 2z_0$ is satisfied. Notice that the curve ($d = 100$ nm, $z_0 = 3$ nm) almost coincides with the $\langle \mathcal{F}^d_{\rm im} \rangle$ curve, since $\langle \mathcal{F}^d_{\rm im} \rangle$, at $z_0 \lesssim 3$ nm, represents the dominant contribution to the total image force for all higher-density electron lattices ($r_0 \lesssim 1000$ nm).

In order to stabilize the Wigner lattice, one can apply an external electrostatic potential giving a constant electric field in the gap $\mathbf{E}_{\rm ex} = E_0\hat{\mathbf{z}}$. This field will press each lattice electron on the He layer with an additional force $\mathcal{F}^e_{\rm ex} = eE_0$, but its effect on the average position z_e of lattice electrons (Fig. 1) can be neglected [16]. Obviously, such a field also pulls together the dielectric plates with a force (per unit area) $\mathcal{F}^d_{\rm ex} = -\epsilon_0 E_0^2/8\pi$. The competition between such a force and some other external forces, like mechanical elastic forces pertinent to the real material, with the Casimir force has been already considered [26].

V. CONCLUSION

In this article we have analyzed a system consisting of an electron lattice in between two metallic or polar dielectric slabs. The main motivation was to take into account two very different manifestations of the electromagnetic field—image potential and Casimir effect—within the same model. As a model which could also serve as an experimental setup we chose a well-known system of quasi-2D Wigner lattice formed above the liquid He layer. We assumed that the lattice is formed as a stable hexagonal configuration, although the specific lattice shape is not important for our discussion, i.e., only a significant lattice parameter is an electron density. The theoretical model is based on the quantum-mechanical description of the electromagnetic field interacting with the electron lattice, as well as with the collective excitations in the slabs. We made some standard approximations that enabled us to present results in a closed form, giving the Casimir effect through the fluctuation of the electromagnetic field in the coherent state, and the electron lattice–metallic (dielectric) slab interaction as the image potential, while the basic properties of the Wigner lattice (the eigenfrequencies) remained essentially unchanged.

It appeared that the Casimir effect could be treated as if the electron lattice is not present in the system. The main effort was to calculate the image potential which was derived in the closed form. For the calculational and interpretational purposes, it was then transformed into the "classical picture" in which each electron in the lattice induces infinite number of images in each slab. We differentiated the "direct images" describing the (attractive) electron interaction with only one slab, and the "induced images" describing the (repulsive) image-image interaction that exists only if both slabs are present. The contribution from the direct images is simple to calculate, while the contribution of induced images was expanded in powers of Ω, where $\Omega = (\omega_L^2 - \omega_T^2)/(\omega_L^2 + \omega_T^2)$ appears to be the only parameter which describes the dielectric properties of the slabs. Such simple description was enabled by neglecting the electronic polarizability of involved media. If needed, the electronic polarizabilities could be introduced in a standard way, but in that case the relevant equations would be much more cumbersome, while the final results, particularly in the case of metallic slabs, would remain almost the same. One can argue that we could take only metallic slabs from the beginning, but besides giving good insight into the dielectric properties of slabs, the parameter Ω was successfully used as expansion parameter and in analytical summations that formally require $\Omega < 1$. However, we can still put $\Omega = 1$ for metallic slabs at the end of our calculations.

The summation over all lattice electrons is performed with the help of Ewald transformation. Since the averaged interaction (the $\mathbf{G} = 0$ term) and therefore the whole image potential diverge, one has to make some regulations to obtain the nondivergent result. For the same reason one has to regulate the Casimir energy. The regulation mechanisms are quite different and there is no point to compare those two energies directly. Therefore, we have discussed the image force instead and compared it with the Casimir force, which did not require any regulation.

There are two types of image forces arising from the image potential—the force acting on the electron lattice and the force acting between the slabs—and we have analyzed both of them. The force on the electron lattice was compared with the force on a single electron, which enabled us to track how the induced image interaction screens the single electron interaction when the (averaged) lattice position z_0 becomes comparable to the lattice parameter r_0. In the $r_0 \ll z_0$ case we are approaching the limit of continuous charge density with zero image force on lattice electrons. That holds only if both slabs are present, regardless of how far they are separated. Consequently, if there is only one slab in the system, it will always attract the electron lattice.

We were particularly interested in the total force acting between the slabs, and the comparison between its image potential and the Casimir part. We have shown that at large slab separations $[d \gg (r_0, z_0)]$ the Casimir force ($\sim 1/d^4$) has negligible contribution to the total force, and the dominant contribution comes from the averaged image interaction, i.e., from the $\mathbf{k} = 0$ component of the image force. This component can be analytically calculated, and it turns out that it does not depend on d, but strongly depends upon electron density ($\sim 1/r_0^4$). Obviously, the parameter r_0 plays a similar role in the averaged image potential as the parameter d does in the Casimir effect; so with the appropriate choice of those parameters one can make the two effects comparable. The third parameter z_0 (position of the lattice) has considerable impact on the image force between the slabs at smaller slab separations ($d < r_0$), but in that case (providing $d > 2z_0$, which is a prerequisite for the lattice formation) the Casimir contribution dominates over the image potential.

We conclude that the total force among the slabs is determined mainly by the Casimir and the averaged image force and therefore can be well estimated without taking into account the specific position z_0 of lattice electrons or the shape of the lattice. We have also estimated critical parameters (r_0^c, d^c) which roughly separate regions with the dominant influence of the image potential ($d \gtrsim d^c$ or $r_0 \lesssim r_0^c$) from that of the Casimir force. In that sense those parameters determine "the meeting point" of the classical and the quantum appearance of the electromagnetic field, and the fine structure constant $\alpha = e^2/\hbar c$ is naturally involved into their definition. Interestingly, the critical parameters are roughly achieved when the distance d between the slabs coincides with the parameter r_0 of the Wigner lattice.

The Wigner lattice of electrons is an interesting system *per se*, but it could be also considered as a model for various molecular layers functionalized with various metallic atoms or radicals with a periodic order that could be used in real functional electromechanical devices and similar nanosized hybrid structures. In those systems the temperature close to zero is not a needed constraint, as in our model with liquid He layer. The characteristic lengths (r_0^c, d^c) of the system we have considered are about the sizes of new emerging electromechanical devices, and the control of the interplay of the two forces, Casimir and image forces, might be of an importance for the proper functioning of the devices. A possible example might be the newly proposed type of low-power, contactless nanoswitches [4], where the change

of the Casimir force with the phase change of the material from amorphous to crystalline form is used. The control of the accompanied buildup of electrostatic charges is of crucial importance in their possible implementation.

ACKNOWLEDGMENTS

This work was supported by the Ministry of Science of the Republic of Croatia under Contract No. 098-0352828-3118.

[1] H. B. G. Casimir, Proc. Kon. Ned. Akad. Wet. **51**, 793 (1948).
[2] P. J. van Zwol, G. Palasantzas, M. van de Schootbrugge, and J. Th. M. De Hosson, Appl. Phys. Lett. **92**, 054101 (2008).
[3] A. Cleland, *Foundations of Nanomechanics* (Springer, New York, 2003).
[4] G. Torricelli, P. J. van Zwol, O. Shpak, C. Binns, G. Palasantzas, B. J. Kooi, V. B. Svetovoy, and M. Wuttig, Phys. Rev. A **82**, 010101(R) (2010).
[5] J. N. Munday, F. Capasso, and V. A. Parsegian, Nature (London) **457**, 1702009; R. Zhao, J. Zhou, Th. Koschny, E. N. Economou, and C. M. Soukoulis, Phys. Rev. Lett. **103**, 103602 (2009).
[6] M. Levin, A. P. McCauley, A. W. Rodriguez, M. T. Homer Reid, and S. G. Johnson, Phys. Rev. Lett. **105**, 090403 (2010); Z. Lenac, Phys. Rev. A **82**, 022117 (2010).
[7] E. Y. Andrei, *Two-Dimensional Electron Systems on Helium and other Cryogenic Substrates* (Kluwer Academic, Dordrecht, 1997).
[8] X. L. Hu and A. J. Dahm, Phys. Rev. B **42**, 2010 (1990).
[9] B. Tanatar and D. M. Ceperley, Phys. Rev. B **39**, 5005 (1989); S. Orozco, R. M. Mendez-Moreno, and M. Moreno, *ibid.* **67**, 195109 (2003).
[10] E. P. Wigner, Phys. Rev. **46**, 1002 (1934).
[11] C. C. Grimes and G. Adams, Phys. Rev. Lett. **42**, 795 (1979).
[12] C. C. Grimes, T. R. Brown, M. L. Burns, and C. L. Zipfeld, Phys. Rev. B **13**, 140 (1976); Z. Lenac and M. Šunjić, *ibid.* **48**, 14496 (1993).
[13] J. M. Kosterlitz and D. J. Thouless, J. Phys. C **6**, 1181 (1973); F. M. Peeters and P. M. Platzman, Phys. Rev. Lett. **50**, 2021 (1983); Z. Lenac and M. Šunjić, Phys. Rev. B **52**, 11238 (1995).
[14] Z. Lenac, Phys. Rev. A **68**, 063815 (2003).
[15] R. J. Glauber and M. Lewenstein, Phys. Rev. A **43**, 467 (1991).
[16] Z. Lenac and M. Šunjić, Phys. Rev. B **43**, 6049 (1991); **46**, 7821 (1992).
[17] Z. Lenac, Phys. Rev. B **71**, 035330 (2005).
[18] L. Bonsall and A. A. Maradudin, Phys. Rev. B **15**, 1959 (1977).
[19] G. D. Mahan, Phys. Rev. B **81**, 195318 (2010).
[20] Z. Lenac and M. Šunjić, Nuovo Cimento B **33**, 681 (1976).
[21] M. Bordag, G. L. Klimchitskaya, U. Mohideen, and V. M. Mostepanenko, *Advances in the Casimir Effect* (Oxford University Press, New York, 2009).
[22] E. M. Lifshitz, Zh. Eksp. Teor. Fiz. **29**, 94 (1995) [Sov. Phys. JETP **2**, 73 (1956)].
[23] F. Zhou and L. Spruch, Phys. Rev. A **52**, 297 (1995).
[24] Z. Lenac and M. S. Tomaš, Phys. Rev. A **78**, 023834 (2008).
[25] C. Genet, A. Lambrecht, and S. Reynaud, Ann. Fond. de Broglie **29**, 331 (2004); C. Henkel, K. Joulain, J.-Ph. Mulet, and J.-J. Greffet, Phys. Rev. A **69**, 023808 (2004).
[26] Z.-Y. Tong, H.-M. Deng, S.-M. Quin, and P.-X. Yang, Int. J. Nonlinear Sci. Num. Simulation **9**, 335 (2008); A. Ramezani, A. Alasty, and J. Akbari, Microsyst. Technol. **14**, 145 (2008).